Crystallographic snapshots of the complete reaction cycle of nicotine degradation by an amine oxidase of the MAO family

Galina Kachalova[a], Karl Decker[b], Andrew Holt[c], and Hans D. Bartunik[a1]

[a]Max Planck Unit for Structural Molecular Biology, MPG-ASMB c/o DESY, Notkestrasse 85, 22607 Hamburg, Germany; [b]Institut für Biochemie und Molekularbiologie, Albert-Ludwig University, Stefan-Meier-Strasse 17, 79104 Freiburg i. Br., Germany; [c]Department of Pharmacology, School of Molecular and Systems Medicine, Faculty of Medicine and Dentistry, 9-58 Medical Sciences Building, University of Alberta, Edmonton, AB, T6G 2H7, Canada

[1]To whom correspondence should be addressed. E-mail: bartunik@mpghdb.desy.de

Classification: Biological Sciences, Biochemistry

Abstract

FAD-linked oxidases constitute a class of enzymes which catalyze dehydrogenation as a fundamental biochemical reaction, followed by reoxidation of reduced flavin. Here, we present high-resolution crystal structures showing the flavoenzyme 6-hydroxy-*L*-nicotine oxidase (6HLNO) in action. 6HLNO was trapped during catalytic degradation of the native substrate in a sequence of discrete reaction states corresponding to the substrate-reduced enzyme, a complex of the enzyme with the intermediate enamine product and formation of the final aminoketone product. The inactive *D*-stereoisomer binds in mirror symmetry with respect to the catalytic axis, revealing absolute stereospecificity of hydrogen transfer to the flavin. The structural data suggest deprotonation of the substrate when bound at the active site, an overall binary complex mechanism and oxidation by direct hydride transfer. The amine nitrogen has a critical role in the dehydrogenation step and may activate carbocation formation at the α-carbon via delocalization from the lone pair to σ* C_α-H. Enzymatically assisted hydrolysis of the intermediate product occurs at a remote (P site) cavity. Substrate entry and product exit follow different paths. Structural and kinetic data suggest that substrate can also bind to the reduced enzyme, associated with slower reoxidation as compared to the rate of reoxidation of free enzyme. The results are of general relevance for the mechanisms of flavin amine oxidases.

\body

Introduction

Flavin-dependent amine oxidases take part in a number of cellular processes ranging from degradative metabolism to chromatin remodeling. A large body of work has examined the common kinetic mechanism of flavoprotein oxidases, which includes a reductive half-reaction yielding the oxidized substrate bound to the reduced enzyme and subsequent reoxidation of the enzyme by oxygen in a binary or ternary complex scheme. The mechanism of individual steps remains controversial as discussed in a number of reviews (1-5). Hypotheses put forward for the dehydrogenation step of the catalytic reaction include radical mechanisms involving single-electron transfer from the substrate to the flavin as a first step (6), nucleophilic mechanisms involving an intermediate substrate-flavin adduct (7, 8), a carbanion mechanism (9) and a direct hydride transfer mechanism, which has been established for D-amino-acid oxidase (DAAO) (4, 10, 11). For a number of flavin amine oxidases including DAAO (11), L-amino acid oxidase (LAAO) (12), monoamine oxidase (MAO) (1, 13, 14) and 6HLNO (15), a carbanion mechanism may be excluded as the active sites do not contain residues capable of and properly placed for acid-base catalysis. Most of the investigations of structural mechanisms involved enzymes in unproductive complexes with substrate analogues or inhibitors. Crystallographic studies of amine oxidases under productive oxidizing conditions were reported for *Rhodosporidium toruloides* D-amino-acid oxidase (RgDAAO) (11), porcine kidney D-amino-acid oxidase (PkDAAO) (16) and *Streptomyces coelicolor* alditol oxidase (17). However, substrate and product were found to coexist in the active site and could not be distinguished, despite the high resolution reached in these studies.

Here we describe discrete structural states populated during productive enzymatic turnover in crystalline 6HLNO. The flavoenzyme is a close structural neighbour (15) of human MAO-A and MAO-B. It is involved in the degradation of nicotine in the soil bacterium *Arthrobacter nicotinovorans*, which starts with 6-hydroxylation of the pyridine ring. In a second step, catalyzed by 6HLNO, the pyrrolidine ring of 6-hydroxy-*L*-nicotine (6HLN) is oxidized to 6-hydroxy-*N*-methylmyosmine and cleaved to yield 6-hydroxy-pseudooxynicotine (18) (Fig. 1A). 6HLNO acts with absolute stereospecificity on 6HLN and is competitively inhibited by the antistereomer 6-hydroxy-*D*-nicotine (6HDN). The present paper describes the functioning of 6HLNO in action, based on high-resolution structures trapped during productive turnover of the *L*-substrate. The structural data and studies of steady-state kinetics provide an experimental basis for assessing the structural mechanism of 6HLNO and revisiting the reaction pathway in MAO.

Results

Structures of 6HLNO trapped during enzymatic turnover

Crystal structures of 6HLNO in different reaction states were obtained at high resolution following initiation of the catalytic reaction in the crystalline enzyme and cryo-trapping (Table S1). The structures E-S-P1 and E-S-P2 showed 6HLN bound with full occupancy at the active site, which is located at the interface between the FAD-binding domain and the substrate-binding subdomains S1 and S2 of the 6HLNO subunit, and a further ligand bound with high occupancy at a second, remote site (Figs. 1B, 2-3). The additional ligand was structurally identified as the intermediate 6-hydroxy-*N*-methylmyosmine (P1) in E-S-P1 and as the final product 6-hydroxy-pseudooxynicotine (P2) in E-S-P2. The binding sites of P1 and P2 are located in a ("P site") cavity, which is lined by residues from S1 (81-88, 99-100, 163-167, 195-199) and S2 (300-302, 309-311). It is further lined by one of the acyl chains of the diglycerophospholipid (Fig. 2), which is non-covalently bound to the S1 subdomain of all 6HLNO structures (15). Binding of P1 or P2 to the P site cavity is associated with a movement of the main chain segment 81-85 and a reorientation of the Phe85 ring (Fig. 3A), which opens the cavity toward the protein surface, enabling release of the final product to the solvent at a location close to the subunit-subunit interface of the 6HLNO dimer. A further structure, E-I-P2, was derived from the reaction of the enzyme with a racemic mixture of the *L*-substrate with 6HDN. E-I-P2 contains 6HDN bound at the active site and, in addition, the product P2 resulting from turnover of the contaminating *L*-substrate bound at the P site.

Active site and substrate-binding geometry

The conformation of 6HLN bound at the active site in E-S-P1 (Fig. S1) and E-S-P2, its orientation with respect to the isoalloxazine ring and the contacts with the protein environment are closely similar as in the previously described dithionite-reduced enzyme-substrate complex (E-S; 3K7Q) (15). The pyrrolidine moiety of the substrate is present in a slightly twisted envelope conformation (Fig. 4) with the amine nitrogen N1' in the apex position pointing away from the isoalloxazine ring (distance N1'-C4a about 4.1 Å). Flavin and ligand-binding geometry data are summarized in Table S2. The pyrrolidine C2' carbon, from which the flavin may abstract a hydride, and N1' adopt sp^3 conformations. The bonds N1'-C2' (bond length 1.46 ± 0.02 Å derived from an average over the bond lengths observed in the structures E-S, E-S-P1, E-S-P2 and E-S-I) and C2'-C3' (1.51 ± 0.02 Å) have single-bond character. The distance of the α-carbon from the flavin N5 nitrogen under oxidizing conditions is 3.42 ± 0.05 Å when averaged over the distances observed in E-S-P1 and E-S-P2. The orientation of the substrate with respect to its immediate protein environment is identical, within about 0.1 Å, in E-S-P1 and E-S-P2.

6HLNO also binds the MAO substrates dopamine and serotonin in the active site pocket (Table S3). The observed unproductive binding modes (Fig. S2) are in agreement with the fact that 6HLNO does not catalyze degradation of these substrates (18) and reflect differences in the active site architecture assuring substrate specificity.

Intermediate and final product states

E-S-P1 shows the intermediate product bound with 70% occupancy at the P site (Fig. 3B). P1 exhibits planar geometry of the aromatic pyrrole ring with a double bond between C2' and C3' (bond length 1.32 Å) and a partial double-bond character of the N1'-C2' bond (1.32 Å). The N1' nitrogen forms a fairly strong hydrogen bond with the side chain carboxylate group of Glu300 (bond length 2.6 Å), which further interacts with a water molecule, wat470. The pyrrole ring is in hydrophobic contact to protein residues and the *sn*-2 chain of the diacylglycerophospholipid (distance 3.6 Å between *sn*-2 C36 and C4' of P1). The side chains of Leu198, Phe85 and Tyr311 form a similar hydrophobic cage around the pyridine moiety as the side chains of Leu198, Phe326 and Tyr59 at the substrate-binding site. The pyridine nitrogen N1 is in hydrogen-bonding contact with the main chain carbonyl oxygen of Leu198. The pyridine hydroxyl interacts with the hydroxyl group of Tyr59 via a bridging water, which is part of a network connecting P1 with the N5 nitrogen of the isoalloxazine ring via the side chain of Lys287 (Fig. 2).

The P site cavity of E-S-P2 contains the final product (Fig. 3C), which is characterized by an opened pyrrole ring and an inserted oxygen. The pyridine moiety of P2 (70% occupancy) adopts a closely similar orientation as P1 in E-S-P1. The ketone moiety, Phe85 and Glu300 each exhibit two alternate conformations. The inserted oxygen atom is in contact with a water network interacting with residues of the segment 196-199.

Different channels for entrance and exit

The reaction pathway from the substrate-binding pocket to the P site cavity and the protein surface runs along the S1-S2 interface (Figs. 1B, 2). The observed coexistence of catalytic turnover products bound at the P site with 6HLN bound at the active site reveals that entry of substrate and product exit employ different paths. Different channels for entrance and exit were already proposed for PAO (19). A number of transiently opening entrance pathways may be suggested for 6HLNO including one superimposing on the putative exit channel in PAO.

Enzyme-inhibitor complexes

Complexes of 6HLNO with 6HDN were studied under dithionite-reduced (E-S-I) and oxidizing (E-I-P2) conditions. In E-S-I, 6HDN is bound at the P site (Figs. 3A, D). When compared to the P1-binding geometry, the pyridine ring of 6HDN is rotated by about 110°, and the pyrrolidine ring is remote from the side chain of Glu300. The conformation of the loop

segment 81-85 is similar as in E-S and the structure of the native enzyme (E_{nat}; 3K7M), in which the P site cavity is free of ligands. The contaminating 6HLN is present in the active site pocket exhibiting a closely similar binding geometry as in E-S-P1, E-S-P2 and E-S.

E-I-P2 shows 6HDN bound at the active site (Fig. 4). The C_{α}-H function of the pyrrolidine moiety points toward the flavin N5 atom. The C2'-N5 distance, 3.6 Å, and the angle C2'-N5-N10, 101°, are essentially identical as in E-S. The amine nitrogen of the inhibitor is located opposite the flavin N5 atom (distance 4.1 Å). The pyridine ring adopts a similar orientation and is engaged in similar hydrogen-bonding interactions as the pyridine ring of the *L*-substrate in E-S. The *trans* orientation of the pyridine and pyrrolidine rings in 6HLN changes to *cis* in the bound *D*-stereoisomer, which constitutes the main difference between the observed geometry and a previous theoretical model of 6HDN binding (15). E-I-P2 further contains the product P2 bound with 50% occupancy at the same location in the P site cavity as in E-S-P2.

Flavin geometry and global motions

Binding of 6HLN or 6HDN at the *Re*-face of the FAD is associated with flattening of the isoalloxazine ring and with tilting towards the *Si*-side (Table S2, Fig. S3) accompanied by a displacement of the main chain segment 56-59. E-S-P1 and E-S-P2 closely agree in the conformation of the flavin and its orientation with respect to the protein environment. In both structures, the bending angle is 5°, which is half-way between the bent geometry in E_{nat}, 9°, and the flat coplanarity in E-S. The inclination angle, ε, between the central ring and the bond connecting N10 to the ribitol C1* carbon (Fig. S3B) exhibits substantial variation between a value of 16° in the substrate-reduced complexes E-S-P1 and E-S-P2, 19-20° in the dithionite-reduced complexes E-S and E-S-I, and 23-24° in E_{nat} and E-I-P2 under oxidizing conditions. When the isoalloxazine rings are aligned on N10 and C1*, the change in ε is associated with displacements of N5 by 0.25 Å between E_{nat} and E-S and by 0.52 Å between E_{nat} and E-S-P2 (Figs. S3A, C). For comparison, the isoalloxazine rings in E-S-P1 and E-S-P2 superimpose with RMSD 0.04 Å between the locations of all ring atoms, which provides an estimate of their reproducibility. The reorientational motion of the flavin associated with the change in the N10 conformation appears to function as a molecular switch, which turns on rigid-body motions of the S1 and S2 subdomains relative to each other and to the FAD-binding domain. When E-S-P1 and E-S-P2 (overall RMSD of 0.25 Å between main chain atoms) are compared to E-S-I and E-S (RMSD 0.34 Å), S1 is found to rotate by about 1.5° around an axis passing through the locations of the flavin N5 and N10 atoms, and S2 by about 0.7° around an axis that is perpendicular to the flavin plane and intersects near N10.

Kinetic assays of enzyme activity

Measurement of the catalytic activity of 6HLNO in a peroxidase-coupled fluorescence assay showed substantial deviation from Michaelis-Menten kinetics and a dependence on ionic

strength (Fig. S4). At high ionic strength, the activity decreases at 6HLN concentrations above 1 mM, displaying a pattern of substrate inhibition. At low ionic strength, the activity of 6HLNO increases with increasing substrate concentration. A similar behaviour was observed for MAO-B and was interpreted on the basis of a two-activity kinetic model (20). Initial rate data for oxidation of 6HLN by 6HLNO in 0.1 M Tris buffer, pH 7.5, were fitted to an equation (20) describing substrate turnover following binding to oxidized (E_{ox}) and reduced enzyme (E_{red}) (Fig. S4A). Effects of ionic strength on oxidation of 6HLN by 6HLNO were monitored in 10 mM Tris buffer, pH 7.5, in the presence of 0, 5 mM or 50 mM NaCl and fitted to the same equation (Fig. S4B). Inhibition by 6HDN of the oxidation of 6HLN by 6HLNO was measured in 0.1 M Tris buffer, pH 7.5 (Fig. S4C). Initial rate data were fitted by global nonlinear regression analysis to an equation (Equation S1 in *SI Materials and Methods*) for linear competitive inhibition by ligand binding to the active sites of both E_{ox} and E_{red}. Mean kinetic constants (± SEM) were K_{Mox} = 50.8±3.5 μM; V_{MAXox} = 2.14±0.03 nmol/ng/h; K_{Mred} = 6.72±6.41 mM; V_{MAXred} = 1.98±0.098 nmol/ng/h; K_{Iox} = 443±71 μM; K_{Ired} = 13.8±7.8 mM; global r^2 = 0.974.

Discussion

Enzymatic reaction states and redox-dependent conformational changes

The crystallographic snapshots of the catalytic action of 6HLNO revealed that the overall reaction, which is summarized in a pictorial scheme in Figure S5, involves two different and spatially remote sites within the enzyme subunit. Following dehydrogenation of the tertiary amine substrate at the active site, the resulting intermediate P1 and the final product P2 were observed at the P site located in a cavity near the protein surface. Turnover of 6HLN also occurred when using a racemic mixture with the inhibitor 6HDN under oxidizing conditions. The affinity of the enzyme for binding at the active site appears to be substantially higher for 6HLN as compared to 6HDN, which agrees with kinetic data presented here and elsewhere (18). The structural data suggest that 6HDN can also compete for the P site (E-S-I). However, fitting the kinetic data (Fig. S4C) by an equation considering mixed plus competitive inhibition resulted in a much lower affinity of 6HDN for the P site than for the active site.

The enzymatic reaction is associated with changes in the flavin geometry, which include in particular systematic redox-dependent changes in the conformation of the flavin N10. The hybridization of N10 is predominantly sp^3 under oxidizing conditions. The observed change to a more sp^2-like character in the dithionite-reduced complex is in agreement with NMR chemical shifts (21). Formation of the enzyme-substrate complex in E-S-P1 and E-S-P2 is accompanied by a further change to an essentially planar sp^2 geometry of N10. Hence, turnover to P1 and P2 is followed by binding of substrate to the reduced enzyme. The structures show coexistence of substrate bound to E_{red} at the active site with product bound at the P site, but no evidence for substrate binding at the P site. Taking the structural and kinetic

data together, the substrate inhibition pattern visible in the kinetics at high ionic strength, which probably corresponds to the conditions in the enzyme crystal, is explained by slower reoxidation when substrate binds to E_{red} as compared to the rate of reoxidation of free enzyme (Fig. S5). The incomplete populations observed for P1 and P2 are consistent with partial release of products to the solvent, indicating that substrate binding to E_{red} does not result in a dead-end complex.

The structural data are of high quality, which is apparent from the electron density maps and the reproducibility of protein, FAD and ligand conformations derived from multiple observations. The unambiguous and accurate identification of structural states was facilitated by the occurrence of stepwise enzymatic turnover at two different sites, both exhibiting rather rigid geometries.

Mechanism of substrate dehydrogenation by 6HLNO

The orientation of the *L*-substrate with respect to the FAD cofactor in the substrate-reduced state of 6HLNO fulfills the geometrical requirements for efficient transfer of hydrogen from the α-carbon C2' to the flavin N5. The C2'-N5 distance of 3.4-3.5 Å and the C2'-N5-N10 angle of about 99° are close to the corresponding values in substrate-bound complexes of DAAO (11, 16), for which a direct hydride transfer mechanism has been established.

Favorable orientation of the α-carbon with respect to N5, however, is not sufficient to explain the catalytic functioning of the enzyme. The C_α-H function of the inactive 6HDN, when bound at the active site in E-I-P2, points toward N5 in a similar orientation as observed for the *L*-substrate (Fig. 4). The pyrrolidine rings of the stereoisomers and the locations of the amine nitrogen are mirrored with respect to a plane, which is perpendicular to the isoalloxazine ring and contains the catalytic axis C2'-N5. The strict stereoselectivity of the reaction catalyzed by 6HLNO implies that dehydrogenation critically depends on correct alignment of the C_α-N1' bond with respect to the flavin ring and specifically involves elimination of *L*-hydrogen from C_α. Absolute stereochemistry of the abstraction of a hydrogen atom was also observed for several MAO substrates including dopamine (22). The crystal structures of a number of complexes of amine oxidases with substrates or substrate analogues, including in particular MAO-A (2Z5X, 1O5W), DAAO (1C0P, 1EVI) and LAAO (2JB2), show the C_α-N bond undergoing oxidation in a similar orientation opposite the C4a-C4=O4 locus as in 6HLNO. As previously suggested (23), this structural feature may be a general crucial factor in achieving catalysis.

We propose that the amine nitrogen group affects carbocation formation at the α-carbon of the *L*-substrate through delocalization of the nitrogen lone pair. The length of the C_α-H bond and the puckering of the pyrrolidine ring depend on the orientation of the bond with respect to the lone pair, which partially participates in an antibonding σ* C-H orbital (24-26). This

orientation is *trans* in the *L*-substrate bound to 6HLNO, stabilizing the conformer. Formation of the aromatic ring of the tertiary imine must be preceded by a movement of the pyrrolidine nitrogen into the pyramidal inversion transition state, which is a rapid process and inexpensive in energy as the carbon atoms remain in a puckered conformation (27). The inversion moves the nitrogen closer to the flavin, reducing the N1'-C4a distance from 4.1 Å to a similar value (about 3.3 Å) as in complexes of DAAO with active substrates (1C0P, 1EVI). The movement of the amine nitrogen brings the lone pair close to the flavin ring, enabling direct interaction with π-electron density, which may cause a decrease in the delocalization to the C_α-H bond. Changes in π-electron density upon substrate binding to 6HLNO were derived from NMR data (21). The flat aromatic ring of the intermediate product of the reductive half-reaction forms on hydride transfer from C_α to the flavin N5 nitrogen, which is associated with a change in the hybridization of the carbon atom from sp^3 to sp^2, and a concomitant change of C2'-C3' to a double bond, whereby wat1013 or another water in the network (15) may serve as a base accepting a proton from C3'.

The methylpyrrolidine ring of nicotine is protonated in aqueous solution (28, 29). Deprotonation of the *L*-substrate may occur upon binding at the active site, which is shielded from access by water, and involve a tyrosine, Tyr407, forming the "aromatic cage" (30) together with Trp371 and the isoalloxazine ring. A tyrosine residue at the location of Tyr407 is conserved in the MAO family (Tyr444 in human and rat MAO-A, Tyr435 in human MAO-B and Tyr439 in PAO). The orientation of the *L*-substrate with respect to the protein environment places the amine nitrogen close to Tyr407, which is in hydrogen-bonding contact with the imidazole of His187 and via a bridging water, wat1015, with Oγ of Ser197 (Fig. 4). The pyrrolidine N^+CH_3-H group may interact with the ring hydroxyl of Tyr407 forming a charge-relay system with His187 and Ser197. The *D*-stereoisomer cannot be deprotonated by such a mechanism, as its methyl group is remote from Tyr407 and points toward the Trp371 side chain. In the case of MAO, a cysteine residue (Cys201 in MAO-A and Cys192 in MAO-B) may be involved in deprotonation of the substrate when bound at the active site. Rotation of the side chain of the conserved tyrosine to a different rotamer state moves the ring hydroxyl to a location where it may pass the proton on to the cysteine side chain interacting with a bound water molecule.

Enzymatically assisted hydrolysis and reoxidation of the flavin

The structures of trapped enzymatic reaction states of 6HLNO do not show any evidence for a presence of the intermediate product P1 of the dehydrogenation step inside the substrate-binding pocket. P1 appears to depart rapidly from the active site, probably due to a repulsive interaction with the reduced flavin, suggesting a binary complex (ping-pong) mechanism of the overall reaction, possibly with alternate pathways for reoxidation of the reduced enzyme (Fig. S5). Modeling of P1 into the active site pocket indicates a steric clash between the

hydroxyl groups of the pyridine moiety and Tyr311 (Fig. S6). The resulting reorientation of the Tyr311 side chain may trigger coordinated motions of the side chains of Tyr59 and Leu198 opening a channel for transfer of P1 to the P site (Fig. 1B). The second step in the reaction, hydrolysis of the P1 intermediate, previously was expected to occur spontaneously and non-enzymatically (18). The observation of both P1 and P2 in discrete and highly populated structural states (Figs. 3B, C) revealed that the opening of the pyrrole ring of the enamine and insertion of an oxygen atom to form the final ketone product P2 in fact take place in the P site cavity of the enzyme. The structural data suggest a principal role of a glutamate residue, Glu300, which may orient and activate a hydrogen-bonded water molecule, possibly wat470 (distance 2.75 Å from the side chain carboxyl of Glu300 and 5.1 Å from C2' of P1), for nucleophilic attack on the pyrrole ring of P1. The pKa of Glu300 may be raised in its hydrophobic environment formed by Phe85, Phe88, Trp163 and Val302.

The presence of the reduced state of the enzyme in E-S-P1 and E-S-P2 may indicate that reoxidation of flavin occurs after product release to the solvent, implying that access of dioxygen upon substrate binding may involve the P site cavity. One of the xenon sites derived from diffraction analysis of 6HLNO under Xe pressure (15) indeed is located close to the site of the P1/P2 pyridine hydroxyl. A possible path runs from this site to a cavity lined by the side chains of Tyr59, Tyr313 and Ala58, which exhibit substantial conformational flexibility when comparing E-S-P1 and E-S-P2 to E_{nat}, and continues to a site near the flavin atoms N5 and C4a. A further xenon site located in the vicinity of the Trp371 ring and the dimethylbenzene moiety of the flavin may be related to an alternate dioxygen access path, which might be employed when substrate is absent from the active site pocket. The C4a carbon has been suggested on the basis of MD calculations for alditol oxidase (31) and isotope effect studies performed on glucose oxidase (32) to be the locus directly involved in electron transfer from the reduced cofactor to O_2. Wat1008, which bridges between Lys287 and the flavin N5 nitrogen in 6HLNO (Figs. 2, S6), may have a role in oxygen activation involving replacement of the water molecule by oxygen and superoxide formation, similar to the process occurring in sarcosine oxidase (33).

Structural interactions of active site residues with residues lining the P site cavity and a network of bound waters connecting both sites (Fig. 2) suggest regulation of the catalytic activity by ligand binding to the P site, in contrast to a ternary complex mechanism proposed for DAAO and MAO, whereby rate constants are increased by product binding at the active site (34).

The structural similarity between MAO and 6HLNO raises the question of whether enzymatically assisted hydrolysis of the imine product may also occur in MAO. The P site cavity of 6HLNO superimposes on the "entrance cavity" of nearly identical volume, which is present in MAO-A and MAO-B (1, 35). Comparative modeling suggests that a cystine, formed

by Cys321 and Cys323, in MAO-A and Cys312 or a glutamate, Glu84, in MAO-B may have a role in activating water for nucleophilic attack and formation of the final product (Fig. S7).

Conclusions

The observation of discrete and well-defined structural states populated during enzymatic turnover catalyzed by 6HLNO provides new insight into the functioning of flavin-dependent amine oxidases of the MAO family, which share closely similar overall structures and active site architectures. A number of new aspects are introduced including the observation that dehydrogenation at the active site is followed by rapid transfer of the imine product to the remote P site cavity, where enzymatically assisted hydrolysis takes place yielding the final product. The corresponding ("entrance") cavity in MAO may have a similar role. The docking models proposed for binding of imines at the P site cavity of MAO involve locations close to the observed imidazoline I_2 binding site in MAO-B (20). A further unexpected result is the structural evidence derived from the conformation of the flavin N10 nitrogen as a marker for reduced/oxidized flavin, for binding of substrate to reduced enzyme. This observation is consistent with kinetic data for 6HLNO suggesting an alternate reoxidation scheme. The structural and kinetic data taken together further support previous proposals of similar schemes for MAO-A (36) and MAO-B (20).

A more general feature shared by amine oxidases of the MAO and DAAO families is the orientation of the vector defined by the α-carbon and the amine nitrogen with respect to the flavin N5 and C4a atoms. This geometry is related to the stereospecificity of hydrogen transfer and a critical role of the amine nitrogen as an activating group, possibly functioning by facilitating carbocation formation via a change in delocalization from the lone pair to the σ* C_α -H orbital. The present results confirm chemically enforced local symmetry between enantiomeric substrate binding geometries as a universal feature in flavoenzymes (12, 15, 37).

The role of the phospholipid bound to 6HLNO remains open to question. The acyl chains may restrain the amplitudes of relative domain motions associated with redox-dependent conformational changes. The known MAO structures contain open hydrophobic channels in the S1 subdomain and exhibit substantial domain motions. Stabilization of the interfaces in MAO may have a role in catalytic reactions and be achieved through interactions of the substrate-binding subdomains with the lipid bilayer.

Materials and Methods

All experiments were carried out using His-tagged 6HLNO. Enzymatic turnover was initiated by soaking enzyme crystals with the substrate under anaerobic conditions and subsequent exposure to oxygen. The catalytic reaction was stopped by shock-freezing at 100 K in a nitrogen gas stream after time intervals ranging from about five to thirty seconds, immediately followed by diffraction data collection. The structures of 6HLNO complexes were determined using the structure of the native enzyme (3K7M), which was solved previously at 1.95 Å resolution on the basis of MAD phasing (15), as a starting model. Data collection and refinement statistics are listed in Tables S1, S3. Similar as in the case of 3K7M and 3K7Q (15), all presently described high-resolution structures show the protein and the FAD cofactor in well-defined electron density (Figs. S3, S8). Pictures were produced with PyMOL (http://pymol.sourceforge.net/). Substrate and inhibitor kinetics were measured in a continuous peroxidase-coupled assay of H_2O_2 generation. Please see *SI Materials and Methods* for more details.

Acknowledgements

We thank Birgitta Fried for skillful technical assistance to the biochemical preparations and the crystallization assays and Prof. Roderich Brandsch for providing samples of 6HLN and 6HDN for kinetic measurements.

References

1. Binda C, Newton-Vinson P, Hubálek F, Edmondson DE, Mattevi A (2002) Structure of human monoamine oxidase B, a drug target for the treatment of neurological disorders. *Nat. Struct. Biol.* 9: 22-26.

2. Ghisla S, Massey V (1989) Mechanisms of flavoprotein-catalyzed reactions. *Eur. J. Biochem.* 181: 1-17.

3. Scrutton NS (2004) Chemical aspects of amine oxidation by flavoprotein enzymes. *Nat. Prod. Rep.* 21: 722-730.

4. Fitzpatrick PF (2003) Carbanion versus hydride transfer mechanisms in flavoprotein-catalyzed dehydrogenations. *Bioorg. Chem.* 32: 125-139.

5. Fitzpatrick PF (2010) Oxidation of amines by flavoproteines. *Arch. Biochem. Biophys.* 493: 13-25.

6. Silverman RB (1995) Radical ideas about monoamine oxidase. *Acc. Chem. Res.* 28: 335-342.

7. Brown LE, Hamilton GA (1970) Some model reactions and a general mechanism for flavoenzyme-catalyzed dehydrogenations. *J. Am. Chem. Soc.* 92: 7225-7227.

8. Edmondson DE, Binda C, Mattevi A (2007) Structural insights into the mechanism of amine oxidation by monoamine oxidases A and B. *Arch. Biochem. Biophys.* 464: 269-276.

9. Walsh CT, Krodel E, Massey V, Abeles RH (1973) Studies on the elimination reaction of D-amino acid oxidase with α-amino-β-chlorobutyrate. *J. Biol. Chem.* 6: 1946-1955.

10. Harris CM, Pollegioni L, Ghisla S (2001) pH and kinetic isotope effects in D-amino acid oxidase catalysis – Evidence for a concerted mechanism in substrate dehydrogenation via hydride transfer. *Eur. J. Biochem.* 268: 5504-5520.

11. Umhau S *et al.* (2000) The X-ray structure of D-amino acid oxidase at very high resolution identifies the chemical mechanism of flavin-dependent substrate dehydrogenation. *Proc. Natl. Acad. Sci.* USA 97: 12463-12468.

12. Pawelek PD *et al.* (2000) The structure of L-amino acid oxidase reveals the substrate trajectory into an enantiomerically conserved active site. *EMBO J.* 19: 4204-4215.

13. Ma J *et al.* (2004) Structure of rat monoamine oxidase A and its specific recognitions for substrates and inhibitors. *J. Mol. Biol.* 338: 103-114.

14. De Colibus L *et al.* (2005) Three-dimensional structure of human monoamine oxidase A (MAO A): relation to the structures of rat MAO A and human MAO B. *Proc. Natl. Acad. Sci.* USA 102: 12684-12689.

15. Kachalova GS *et al.* (2010) Crystal structure analysis of free and substrate-bound 6-hydroxy-*L*-nicotine oxidase from *Arthrobacter nicotinovorans*. *J. Mol. Biol.* 396: 785-799.

16. Mizutani H *et al.* (2000) Three-dimensional structure of purple intermediate of porcine kidney D-amino acid oxidase. Optimization of the oxidative half-reaction through alignment of the product with reduced flavin. *J. Biochem.* 128: 73-81.

17. Forneris F *et al.* (2008) Structural analysis of the catalytic mechanism and stereoselectivity in *Streptomyces coelicolor* alditol oxidase. *Biochemistry* 47: 978-985.

18. Decker K, Dai VD (1967) Mechanism and specificity of *L*- and *D*-6-hydroxynicotine oxidase. *Eur. J. Biochem.* 3: 132-138.

19. Binda C *et al.* (1999) A 30 Å long U-shaped catalytical tunnel in the crystal structure of polyamine oxidase. *Structure* 7: 265-276.

20. McDonald GR, Olivieri A, Ramsay RR, Holt A (2010) On the formation and nature of the imidazoline I_2 binding site on human monoamine oxidase-B. *Pharmacol. Res.* 62: 475-488.

21. Pust S, Vervoort J, Decker K, Bacher A, Müller F (1989) ^{13}C, ^{15}N, and ^{31}P NMR studies on 6-hydroxy-L-nicotine oxidase from *Arthrobacter oxidans*. *Biochemistry* 28: 516-521.

22. Yu PH, Bailey BA, Durden DA, Boulton AA (1986) Stereospecific deuterium substitution at the alpha-carbon position of dopamine and its effect on oxidative deamination catalyzed by MAO-A and MAO-B from different tissues. *Biochem. Pharmacol.* 35: 1027-1036.

23. Binda C, Newton-Vinson P, Hubálek F, Edmondson DE, Mattevi A (2001) Structure of human monoamine oxidase B, a drug target for the treatment of neurological disorders. *Nat. Struct. Biol.* 9: 22-26.

24. Carballeira L, Pérez-Juste I (1998) Ab initio study of the pseudorotation and conformational stability of pyrrolidine. J. Chem. Soc., *Perkin Trans.* 2: 1339-1345.

25. Schäfer L, van Alsenoy C, Williams JO, Scarsdale JN, Geise HJ (1981) Ab initio studies of structural features not easily amenable to experiment: Part 8. The structural consequences of the anomeric effect in compounds with disubstituted tetrahedral carbon atoms. *J. Mol. Struct.* (THEOCHEM) 76: 349-361.

26. Krueger PJ, Jan J, Wieser HJ (1970) Infrared spectra: intramolecular *trans* lone pair interaction with α-CH bonds and the stability of conformers in alcohols and thiols. *Mol. Struct.* 5: 375-387.

27. Huang X, Zheng F, Crooks PA, Dwoskin LP, Zhan CG (2005) Modeling multiple species of nicotine and deschloroepibatidine interacting with α4β2 nicotinic acetylcholine receptor: From microscopic binding to phenomenological binding affinity. *J. Am. Chem. Soc.* 127: 14401-14414.

28. Graton J *et al.* (2002) Site of protonation of nicotine and nornicotine in the gas phase: pyridine or pyrrolidine nitrogen. *J. Am. Chem. Soc.* 124: 10552-10562.

29. Elmore DE, Dougherty DA (2000) A computational study of nicotine conformations in the gas phase and in water. *J. Org. Chem.* 65: 742-747.

30. Li M, Binda C, Mattevi A, Edmondson DE (2006) Functional role of the „aromatic cage" in human monoamine oxidase B: structures and catalytic properties of Tyr435 mutant proteins. *Biochemistry* 45: 4775-4784.

31. Baron R *et al.* (2009) Multiple pathways guide oxygen diffusion into flavoenzyme active sites. *Proc. Natl. Acad. Sci.* USA 106: 10603-10608.

32. Roth JP *et al.* (2004) Oxygen isotope effects on electron transfer to O_2 probed using chemically modified flavins bound to glucose oxidase. *J. Am. Chem. Soc.* 126: 15120-15131.

33. Zhao G, Bruckner RC, Jorns MS (2008) Identification of the oxygen activation site in monomeric sarcosine oxidase: role of Lys265 in catalysis. *Biochemistry* 47: 9124-9135.

34. Mattevi A (2006) To be or not to be an oxidase: challenging the oxygen reactivity of flavoenzymes. *Trends Biochem. Sci.* 31: 276-283.

35. Edmondson DE, Binda C, Mattevi A (2007) Structural insights into the mechanism of amine oxidation by monoamine oxidases A and B. *Arch. Biochem. Biophys.* 464: 269-276.

36. Ramsay RR (1991) Kinetic mechanism of monoamine oxidase A. *Biochemistry* 30: 4624-4629.

37. Mattevi A *et al.* (1996) Crystal structure of D-amino acid oxidase: a case of active site mirror-image convergent evolution with flavocytochrome b_2. *Proc. Natl. Acad. Sci.* USA 93: 7496-7501.

Figure Legends

Fig. 1. Reaction catalyzed by 6HLNO. (A) Dehydrogenation of the pyrrolidine moiety of 6HLN (S) results in the formation of the intermediate product 6-hydroxy-N-methylmyosmine (P1). Subsequent hydration of the intermediate opens the pyrrole ring to form the final product 6-hydroxy-pseudooxynicotine (P2). (B) Crystal structure of 6HLNO subunit with substrate and product sites. 6HLN (teal) is bound at the active site and the intermediate product P1 (orange) at the P site. PHL denotes a non-covalently bound phospholipid. The insert shows the

solvent-inaccessible active site cavity (yellow; volume 195 $Å^3$), the exit (P site) cavity (brown; 290 $Å^3$) opening toward the protein surface and the channel (red; 80 $Å^3$) for gated transfer of the intermediate product. Arrows indicate possible paths for entry and exit.

Fig. 2. Enzymatic reaction states populated during catalytic turnover in 6HLNO crystals. Stereoview of E-S-P1 (grey) showing the substrate 6HLN (yellow) bound at the active site and the intermediate product P1 (orange) in the P site cavity. The structure of the dithionite-reduced complex E-S (teal) is superimposed.

Fig. 3. Binding geometry at P site. (A) The structures E-S-P1 (orange), E-S-P2 (green), E-S-I (magenta), E-S (yellow) and E_{nat} (grey) are superimposed. Ligand binding to the P site is associated with backbone motions of the segment 81-85. The orientation in the P site cavity is shown for (B) the intermediate P1 (orange), (C) the final product P2 (green) and (D) the inhibitor 6HDN (magenta). Simulated annealed omit (F_o-F_c) maps are contoured at 2.2 σ for P1, 1.8 σ for P2 and 3.0 σ for 6HDN.

Fig. 4. *L*- and *D*-stereoisomers bound at active site. The structures E-S-P1 (yellow) and E-I-P2 (teal) are superimposed. The pyrrolidine rings of 6HLN and 6HDN are related by an approximate mirror symmetry. The α-carbon hydrogens (grey) occupy closely similar locations. The pyrrolidine N^+CH_3-H group of 6HLN may interact with Tyr407 forming a charge-relay system with His187 and Ser197. The amine nitrogen of 6HLN is located opposite the C4a-C4=O4 locus. The distance between C_α of 6HLN and the flavin N5 is 3.48 Å (pink broken line).

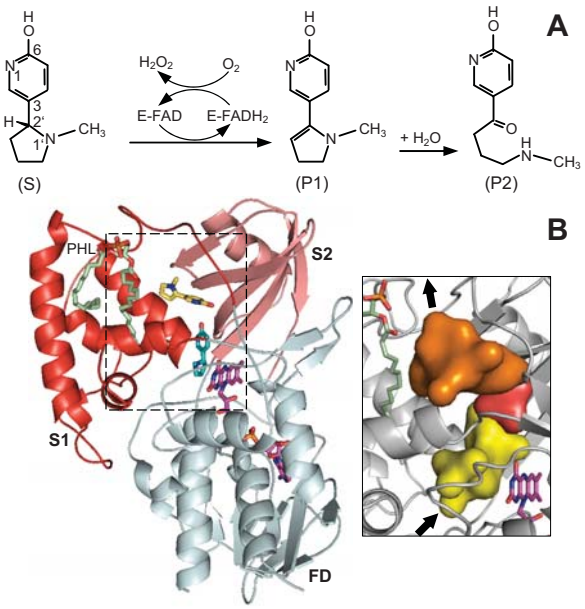
A
H
O
6
N
1
3
H
2'
1'
N
CH3
(S)
H2O2
O2
E-FAD
E-FADH2
(P1)
+ H2O
(P2)
B
PHL
S2
S1
FD

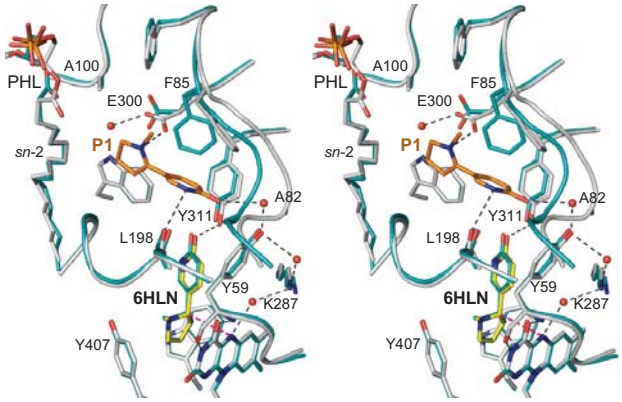
PHL
A100
F85
E300
P1
sn-2
A82
Y311
L198
Y59
K287
6HLN
Y407
PHL
A100
F85
E300
P1
sn-2
A82
Y311
L198
Y59
K287
6HLN
Y407

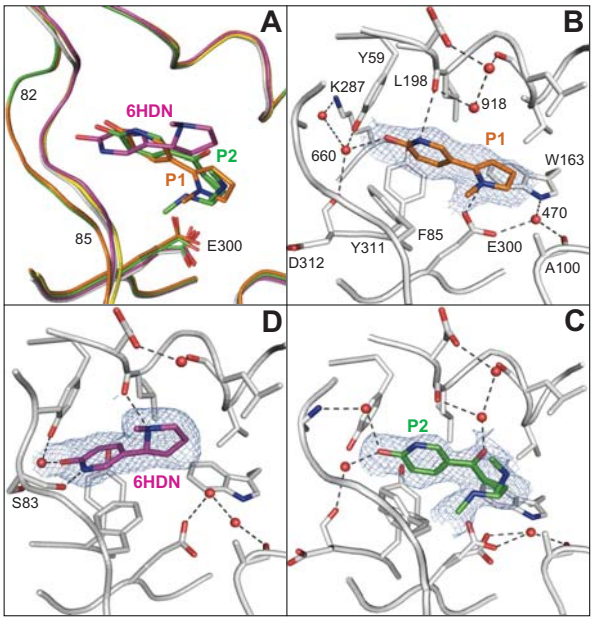
A
82
6HDN
P2
P1
85
E300
B
Y59
K287
L198
918
P1
660
W163
470
F85
Y311
E300
D312
A100
D
6HDN
S83
C
P2

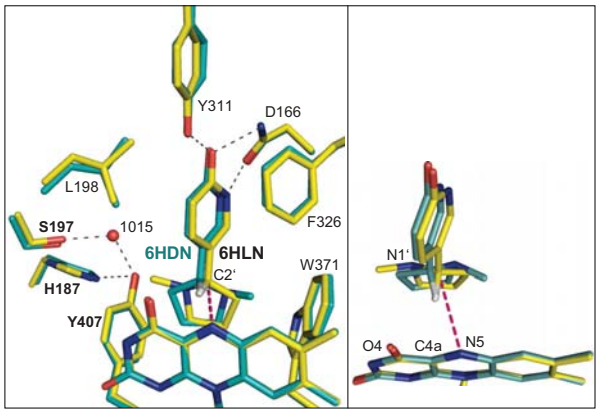
Y311
D166
L198
S197
1015
F326
6HDN
6HLN
W371
C2'
H187
Y407
N1'
O4
C4a
N5